International Journal of Luminescence and applications
Vol6 (4) January, 2017, **ISSN 2277 – 6362**

Enhanced Luminescence on doping of Charge Compensator Ions ($R+ = Li^+$, Na^+ and K^+) in $Ca_2MgSi_2O_7:Eu^{3+}$ Phosphors

Ishwar Prasad Sahu[1*], D.P. Bisen[1], K.V.R. Murthy[2], R.K. Tamrakar[3]

[1]School of Studies in Physics & Astrophysics, Pt. Ravishankar Shukla University, Raipur (C.G.) India
[2]Applied Physics Department, The MS University of Baroda, Vadodara, Gujarat, India
[3]Department of Applied Physics, Bhilai Institute of Technology, Durg (C.G.) India
Corresponding author: ishwarprasad1986@gmail.com

Abstract - *The role of charge compensator ions ($R^+ = Li^+$, Na^+ and K^+) co-doped with Eu^{3+} in di-calcium magnesium di-silicate ($Ca_2MgSi_2O_7$) phosphors were investigated. The $Ca_2MgSi_2O_7:Eu^{3+}$ and $Ca_2MgSi_2O_7:Eu^{3+}$, R^+ ($R^+ = Li^+$, Na^+ and K^+) phosphors were prepared by conventional solid state reaction method. The crystal structures of synthesized phosphors were an akermanite type structure which belongs to the tetragonal crystallography. Thermoluminescence (TL) kinetic parameters such as activation energy, order of kinetics and frequency factor was calculated by peak shape method. The excitation and emission spectra indicate that this phosphor can be excited by near ultraviolet light at 396 nm, and exhibits bright orange – red emission with the highest peak at 595 nm corresponding to the $^5D_0 \rightarrow {}^7F_1$ transition of Eu^{3+} ions. Decay graph indicate that these phosphors also contain fast and slow decay process. CIE color chromaticity diagram confirm that the prepared phosphors would emit orange-red color. The addition of charge compensator ions enhances the luminescence intensity of prepared $Ca_2MgSi_2O_7:Eu^{3+}$ phosphors because they neutralize the charge generated by Eu^{3+} substitution for Ca^{2+} ions. The role of Li^+ ions among all charge compensator ions (Na^+ or K^+) used was found to be most effective for enhanced Eu^{3+} ion emission.*

Keywords: *Alkaline earth silicates; XRD; Photoluminescence; CIE color co-ordinates.*

1. INTRODUCTION

Semiconductor white light-emitting diodes (WLEDs) have emerged as the fourth generation of illumination technology, and are expected to replace the traditional incandescent, fluorescent, and high intensity discharge lamps due to advantages such as energy-saving, long service life, low voltage, high

efficiency, good stability, and adjustable color (1). At present, the common way for manufacturing WLEDs is to combine a blue LED with $Y_3Al_5O_{12}:Ce^{3+}$ phosphor (2). Although this type of WLEDs has a high luminous efficiency, it still reveals a low color rendering index because of deficiency in red light component. The current commercial red phosphor for UV LEDs is $Y_2O_2S:Eu^{3+}$. However, it is chemically unstable due to its sulfide nature, and it is uneconomical to use rare earth oxides (3,4). A red phosphor with high absorption in the near-UV/blue spectral region, that also offers chemical stability and low cost, is urgently needed for UV LEDs. Thus, it is needed to develop more efficient red or orange- red emitting phosphors suitable for the fabrication of WLEDs (5). Compared with sulfide-based phosphors, silicate-based phosphors have been found to be more chemically and thermally stable, and lower in cost. Therefore, in recent years silicate-based luminescent materials have become a research hotspot, and many studies on phosphors with a silicate as the host have been conducted (6,7). Most researchers focus their attention on Eu2+ and Eu3+ ions as the luminescence center in red-emitting phosphors (8).

Generally, phosphors consist of activator and host, in order to obtain efficient red or orange–red emitting phosphor; host is another key factor (9, 10). Mellite are a large group of compounds characterized by the general formula $M_2T^1T^2{}_2O_7$, (M = Sr, Ca, Ba;, T^1 = Mn, Co, Cu, Mg, Zn; T_2 = Si, Ge), have attracted extensive attention as host materials for lanthanide activators because of their excellent physical, chemical, thermal stability and optical property (11, 12). Recently di-calcium magnesium di-silicate ($Ca_2MgSi_2O_7$) phosphor has attracted great interest due to its special structure features, excellent physical and chemical stability. A calcium silicate phosphor would be ideal from the manufacturing point of view, because both calcium and silica are abundant and are relatively inexpensive (13, 14).

Charge compensation is considered an important technique to increase the crystallanity and enhance the emission intensity of phosphors. Many phosphors, having a mismatch in the valency which results in defect formation and acts as a deterrent in the case of emission, are known to be synthesized using charge compensatory additives (15, 16). The subversive nature of the defect causes a detrimental change in the luminescence of the phosphors. Therefore, curbing the phosphor defects and modifying the band gap are an important challenge for achieving high luminescence output (17). Thus, alkali metal ions such as Li^+, K^+, and Na^+ are readily used for local site symmetry modification for improving the luminescence efficiency because these ions have low oxidation states and distinct ionic radii (18-20).

Therefore, in the present work, we report the phosphor synthesis, structural characterization and luminescence properties of $Ca_2MgSi_2O_7:Eu^{3+}$ and $Ca_2MgSi_2O_7:Eu^{3+}$, R^+ phosphors by solid state reaction method. Investigation on the crystal structure was determined by the X-ray diffraction (XRD) techniques. Luminescence properties were also investigated on the basis of Thermoluminescence (TL), Photoluminescence (PL), CIE color coordinates and decay studies. The influence of the charge compensator on the orange-red emission has been studied in detail.

2. EXPERIMENTAL

2.1 Material Preparation

The $Ca_2MgSi_2O_7:Eu^{3+}$ and $Ca_2MgSi_2O_7:Eu^{3+}$, R^+ (R^+ = Li^+, Na^+ and K^+) phosphors were prepared by the traditional high temperature solid state reaction method. The starting materials were strontium carbonate [$CaCO_3$ (99.90%)], magnesium oxide [MgO (99.90%)], silicon di-oxide [SiO_2 (99.99%)] and europium oxide [Eu_2O_3 (99.90%)], all of analytical grade (A.R.), were employed in this experiment. Boric acid (H_3BO_3) was added as flux. The small amounts of flux, improve the phosphors long afterglow, luminescent intensity, reduce the phosphors synthetic temperature, improve the phosphor synthetic quality and increase the production rate. Appropriate amounts of Li_2CO_3, Na_2CO_3 and K_2CO_3 were added as the charge compensator for Eu^{3+} doped samples. Stoichiometrical amount of the raw materials was thoroughly mixed for 2 hour using the mortar and pestle. The ground sample was placed in an alumina crucible and subsequently fired at 1200 ^oC for 3 hour in an air. At last the nominal compounds were obtained after the cooling down of programmable furnace and products were finally ground into powder for characterizing the phosphors.

2.2 Measurement Techniques

The crystal structures of the sintered phosphors were characterized by powder XRD analysis. Powder XRD pattern has been obtained from Bruker D8 advanced X-ray powder diffractometer and the data were collected over the 2θ range 10^o-80^o. The X-rays were produced using a sealed tube (CuKα) radiation source and the wavelength of X-ray was 1.54060 Å. The X-rays were detected using a fast counting detector based on silicon strip technology (Bruker LynxEye detector). The crystal structure of the sample was verified with the help of Joint Committee of Powder Diffraction Standard Data (JCPDS) file. TL glow curve was recorded with the help of TLD reader 1009I by Nucleonix (Hyderabad,

India Pvt. Ltd.) and the uncertainty value of the temperature was +/- 1K. Every time for the TL measurement, the quantity of the powder samples were kept fixed (8 mg). The excitation and emission spectrum was recorded on a Shimadzu (RF 5301-PC) spectrofluorophotometer using the Xenon lamp (150 W) as excitation source when measuring. The color chromaticity coordinates were obtained according to CIE 1931. The decay curves were obtained using a Perkin Elmer fluorescence spectrometer with the proper excitation under a UV lamp (365 nm). All measurements were carried out at the room temperature.

3. RESULTS AND DISCUSSION

3.1 XRD analysis

Measurements of X-ray diffraction of all powder samples were performed to verify the phase purity and to check the crystal structure. Fig. 1(a) shows the XRD patterns of $Ca_2MgSi_2O_7$, $Ca_2MgSi_2O_7:Eu^{3+}$ and $Ca_2MgSi_2O_7:Eu^{3+}$, R^+ phosphors with the Joint Committee of Powder Diffraction Standard Data file (JCPDS: 77-1149) (21). All the diffraction peaks of the resultant phosphors were consistent with JCPDS file and all the compositions show single phase formation. No impurity phase has been observed in any of the compositions, clearly suggesting that the activator and charge compensator ions (Eu^{3+} and R^+) have been incorporated in the lattice. The dopants do not induce a significant change of the crystalline structure of $Ca_2MgSi_2O_7$ composition. Considering the effect of ionic sizes of cations, we propose that Eu^{3+} are expected to preferably occupy the Ca^{2+} (1.12 Å) sites, because of the ionic radii of Eu^{3+} (1.07 Å). The crystal of the sintered phosphor was akermanite type structure which belongs to the tetragonal crystallography with space group $P\bar{4}2_1m$ (113 space number and D^3_{2d} space group), this structure is a member of the melilite group and forms a layered compound.

In order to obtain the crystallographic parameters of the sample, powder X ray diffraction spectrum was analyzed by Rietveld fitting method. Fig. 1 (b) gives the comparison between observed, calculated and standard (COD card No. 96-900-6938) XRD pattern of $Ca_2MgSi_2O_7:Eu^{3+}$, Li^+ phosphor. The Standard XRD pattern of $Ca_2MgSi_2O_7$ (COD card No. 96-900-6938) seems to show quite similar pattern as observed. Figure of merit while matching observed and standard XRD pattern was 0.9356 which illustrate that phase of prepared sample agrees with the standard pattern COD card No. 96-900-6938. The pattern is characterized by few prominent peaks found at different glancing angles (22).

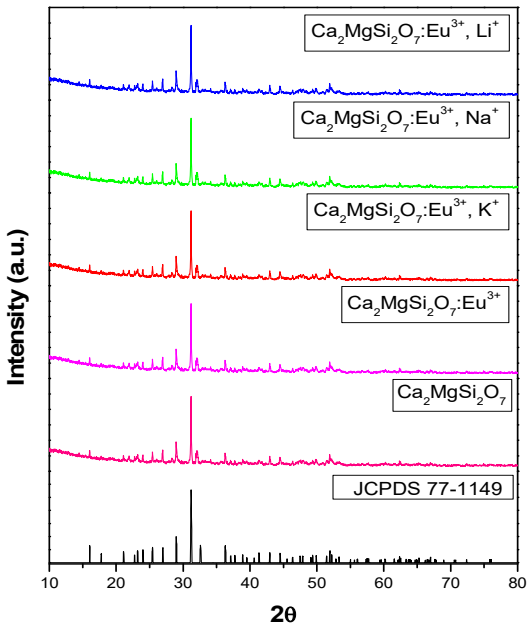

Fig. 1 (a) XRD patterns of $Ca_2MgSi_2O_7$, $Ca_2MgSi_2O_7:Eu^{3+}$ and $Ca_2MgSi_2O_7:Eu^{3+}$, R^+ phosphors with JCPDS file

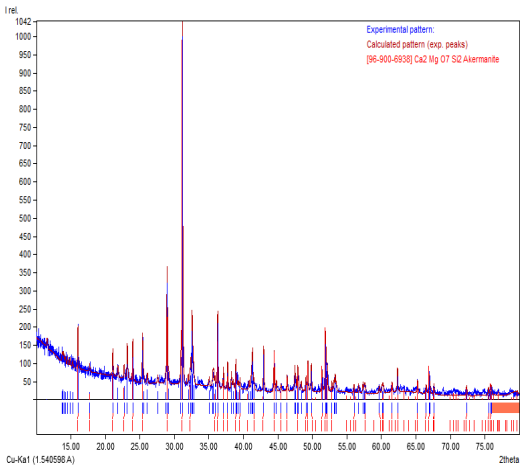

Fig. 1(b) Observed, calculated and standard XRD pattern of $Ca_2MgSi_2O_7:Eu^{3+}$, Li^+ phosphor

The calculated XRD pattern confirmed the presence of tetragonal $Ca_2MgSi_2O_7$. The indexing and refinement of lattice parameters were done using software Celref Version 3 (23). The refined values of tetragonal $Ca_2MgSi_2O_7:Eu^{3+}$, Li^+ phosphor was found as; a = b = 7.8428 Å, c = 5.0053 Å, $\alpha = 90^o$, $\beta = 90^o$, $\gamma = 90^o$ and cell volume = 307.9 $(Å)^3$ which again signifies the proper preparation of the discussed $Ca_2MgSi_2O_7:Eu^{3+}$, Li^+ phosphor.

3.2 Thermo luminescence (TL)

Thermo luminescence (TL) is a good way to detect the combination emission caused by thermal de-trapping of carriers. To get TL emission from a material three essential conditions are necessary. Firstly the material must be an insulator or a semiconductor. Secondly the material should have some time-absorbed energy during exposure to radiation. Thirdly heating the material triggers the luminescent emission (24). Once TL emission has been observed the material will not show it again after simply cooling the specimen and reheating it but has to be exposed to radiation to obtain TL again. What has to be emphasized is that traps and carriers (electrons and holes) may be produced by irradiation, but they are also to be created during sample processing. The plot of intensity of the emitted light against temperature is known as glow curve (25).

In order to study the trap states of the prepared $Ca_2MgSi_2O_7:Eu^{3+}$ and $Ca_2MgSi_2O_7:Eu^{3+}$, R^+ phosphors, TL glow curves were recorded and are shown in Fig. 2(a). The sintered phosphors were first irradiated for 10 min using 365 nm UV source, then the radiation source was removed and the irradiated samples were heated at a linear heating rate of 5°C/s, from room temperatures to 300°C. Initially the TL intensity increases with temperature, attains a peak value for a particular temperature, and then it decreases with further increase in temperature. A single glow peak of $Ca_2MgSi_2O_7:Eu^{3+}$ and $Ca_2MgSi_2O_7:Eu^{3+}$, R^+ phosphors were obtained at 159 °C, indicating that the electron traps involved are deep enough and high energy was required to release the trapped electrons; hence long storage of trapped charge carriers at normal working temperature was achieved and thus the thermal stability was ensured. The single isolated peak due to the formation of only one type of luminescence center which was created due to the UV irradiation. It is suggested that the recombination center associated with the glow at the temperature interval arises from the presence of liberated pairs, which are probably the results from the thermal release of electron/holes from electron/hole trap level and recombine at the color centers. It is also known that the doping of the rare earth ions increases the lattice defects which have existed already in the host. The TL kinetic parameters were calculated and listed in Table 1.

Fig. 2(b) shows the TL emission spectra of $Ca_2MgSi_2O_7:Eu^{3+}$, Li^+ phosphor. TL emission spectra of $Ca_2MgSi_2O_7:Eu^{3+}$, Li^+ phosphor shows broad peak around 600 nm corresponds to orange-red color in the visible region. From, TL emission spectra of $Ca_2MgSi_2O_7:Eu^{3+}$, Li^+ and phosphor confirms single isolated peak due to the formation of only one type of luminescence center which is created due to the UV irradiation.

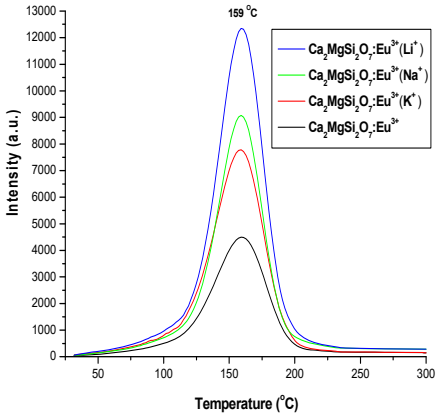

Fig. 2 (a) TL glow curve of $Ca_2MgSi_2O_7:Eu^{3+}$ and $Ca_2MgSi_2O_7:Eu^{3+}$, R^+ phosphors for 10 min UV irradiation

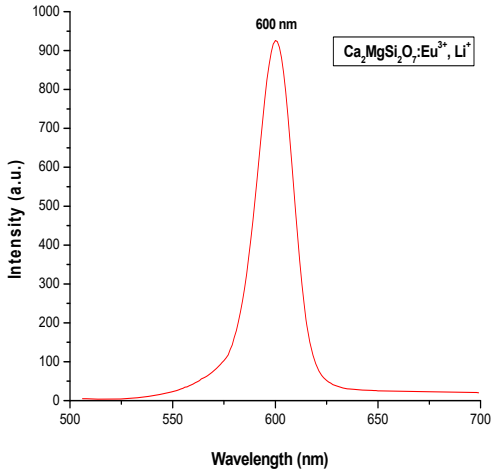

Fig. 2(b) TL emission spectra of $Ca_2MgSi_2O_7:Eu^{3+}$, Li^+ phosphor

3.3 Determination of kinetic parameters

The TL emission characteristic of a phosphor material mainly depends on the kinetic parameters describing the trapping-emitting centers which are quantitatively responsible. For example, the estimation of the time elapsed since exposure is closely related to the position of the trapping levels (E) within the band gap and frequency factor (s) of the electrons in the traps and therefore it is necessary to have a good knowledge of these parameters. There are various methods for evaluating the trappin g parameters from TL glow curves (26).

Evaluation of kinetic parameters, associated with the glow peaks of the thermally stimulated

luminescence, is one of the most studied subjects in the field of condensed matter physics and a complete description of the thermoluminescent characteristics of a TL material requires obtaining these parameters. There are various methods for evaluating the trapping parameters from TL glow curves. For example, when one of the TL glow peaks is highly isolated from the others, the experimental method such as peak shape method is a suitable method to determine kinetic parameters. The TL parameters for the prominent glow peaks of prepared phosphor were calculated using the peak shape method (27).

Glow curve peak shape method: Using the glow curve peak shape method the different shape parameters of the phosphors namely the total half intensity $\omega = T_2 - T_1$ ($\tau+\delta$), τ is the half width at the low temperature side of the peak or the low temperature half width ($\tau = T_m - T_1$); δ is the half width towards the fall-off side of the glow peak or the high temperature half width ($\delta = T_2 - T_m$), and T_m is the peak temperature and T_1 and T_2 are temperature on either side of T_m corresponding to half peak intensity were determined and presented in Table 2. Fig. 3 shows the schematic diagram of glow curve peak shape method (28).

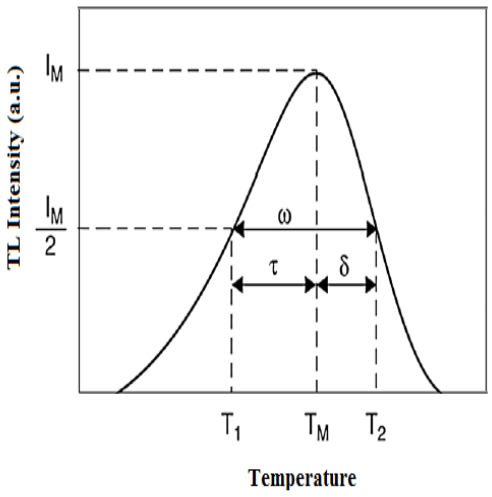

Fig. 3 Schematic diagram of glow curve peak shape method

Order of kinetics (*b*): The mechanism of recombination of de-trapped charge carriers with their counterparts is known as the order of kinetics (*b*). The order of kinetics can be predicted from shape of glow curve by using symmetry factor or geometric factor (μ_g) stated by Chen can be given as

$$\mu_g = \delta/\omega = T_2 - T_m / T_2 - T_1 \qquad (1)$$

The symmetry factor is to differentiate between first and second order TL glow peak. (μ_g) = 0.39-0.42 for the first order kinetics; (μ_g) = 0.49-0.52 for the second order kinetics and (μ_g) = 0.43-0.48 for the mixed order of kinetics.

Activation energy (E): The knowledge about trapping parameters for calculating trap information in traps centre such as required energy for escaping one electron from trap centre known as activation energy or trap depth "E". So, the trap depth calculated by different methods proposed by several authors (29). Trap depth for second order kinetics is calculated using the equation (2)

$$E = 2kT_m\left(1.76\,\frac{T_m}{\omega} - 1\right) \qquad (2)$$

Where, k is Boltzmann constant, E is activation energy; T_m is temperature of peak position.

Frequency factor (s): Frequency factor reflects the probability to escape of electrons from the traps after exposure of ionizing radiation and it is one of the important parameter of the phosphor characterization. Once the order of kinetics and activation energy were determined, the frequency factor (s) can be calculated from the equation (3)

$$\frac{\beta E}{kT_m^{\,2}} = s\left[1 + (b-1)\frac{2kT_m}{E}\right]\exp(E/KT_m) \qquad (3)$$

Where b is order of kinetics, and β is the heating rate. In the present work $\beta = 5^oCs^{-1}$.

The calculated kinetic parameters of $Ca_2MgSi_2O_7:Eu^{3+}$ and $Ca_2MgSi_2O_7:Eu^{3+}$, R^+ phosphors by the peak shape method was given in Table 2. In our case, the value of shape factor (μ_g) was estimated to range between 0.47 to 0.49, which indicates that it is a case of mixed (intermediate) order kinetics, approaching towards second order, responsible for deeper trap depth (30), the activation energy for prepared $Ca_2MgSi_2O_7:Eu^{3+}$ and $Ca_2MgSi_2O_7:Eu^{3+}$, R^+ phosphors were > 1.10 eV.

Table 2 Activation Energy (E), Shape factor (μ_g) and Frequency Factor (s^{-1}) for 10 minute UV irradiated $Ca_2MgSi_2O_7:Eu^{3+}$ and $Ca_2MgSi_2O_7:Eu^{3+}$, R^+ phosphors

τ	δ	ω	μ = δ/ω	E	s
24.90	22.20	47.10	0.47	1.12	6.64×10^{12}
24.80	22.00	46.80	0.47	1.13	8.23×10^{12}
22.50	20.50	43.00	0.48	1.24	1.59×10^{14}
21.00	19.80	40.80	0.49	1.31	1.13×10^{15}

Phosphors Name	UV Min	HTR	T_1 (°C)	T_m (°C)	T_2 (°C)
$Ca_2MgSi_2O_7:Eu^{3+}$	10	5	134.1	159	181.2
$Ca_2MgSi_2O_7:Eu^{3+}(K^+)$	10	5	134.2	159	181.0
$Ca_2MgSi_2O_7:Eu^{3+}(Na^+)$	10	5	136.5	159	179.5
$Ca_2MgSi_2O_7:Eu^{3+}(Li^+)$	10	5	138.0	159	178.8

3.4 Photoluminescence (PL)

The excitation spectrum of $Ca_2MgSi_2O_7:Eu^{3+}$ and $Ca_2MgSi_2O_7:Eu^{3+}$, R^+ (R^+ = Li^+, Na^+ and K^+) phosphors were excited at 396 nm was shown in Fig. 4 (a). It can be seen that its emission spectra are all composed of several sharp lines from the characteristic Eu^{3+} emission. The excitation spectrum of $Ca_2MgSi_2O_7:Eu^{3+}$ and $Ca_2MgSi_2O_7:Eu^{3+}$, R^+ phosphors were exhibited a broad band in the UV region centered at about 242 nm, and several sharp lines between 300 to 400 nm. Eu^{3+} ions has a $4f^6$ configuration, it needs to gain one more electron to achieve the half-filled $4f^7$ configuration, which is relatively stable compared to partially filled configurations (31). When Eu^{3+} is linked to the O ligand, there is a chance of electron transfer from O to Eu^{3+} to form $Eu^{2+} - O^2$ (simply Eu–O). During this, there is a broad absorption band at 230 – 280 nm, depending on the host. This is known as the Eu–O charge transfer band (CTB).

It can be seen from Fig. 4 (a), the excitation spectrum is composed of two major parts: (1) the broad band between 220 and 300 nm, the broad absorption band is called charge transfer state (CTS) band due to the europium-oxygen interactions, which is caused by an electron transfer from an oxygen 2p orbital to an empty 4f shell of europium and the strongest excitation peak at about 242 nm. (2) A series of sharp lines between 300 to 500 nm, ascribed to the f-f transition of Eu^{3+} ions. The sharp peak is located at 396 nm corresponding to $^7F_0 \rightarrow {}^5L_6$ transition of Eu^{3+}. Other weak excitation peaks are located at 320, 328, 348, 363, 384, 416 and 466 nm are related to the intra-configurational 4f–4f transitions of Eu^{3+} ions in the host lattices. The prepared $Ca_2MgSi_2O_7:Eu^{3+}$ and $Ca_2MgSi_2O_7:Eu^{3+}$, R^+ phosphors can be excited by near UV (NUV) at about 396 nm effectively. So, it can match well with UV and NUV-LED, showing a great potential for practical applications (32).

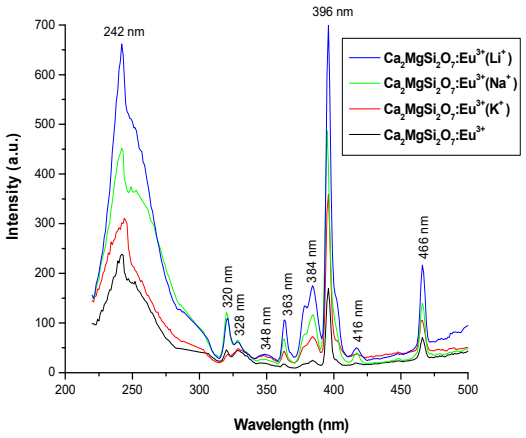

Fig. 4 (a) Excitation spectra of $Ca_2MgSi_2O_7:Eu^{3+}$ and $Ca_2MgSi_2O_7:Eu^{3+}$, R^+ phosphors

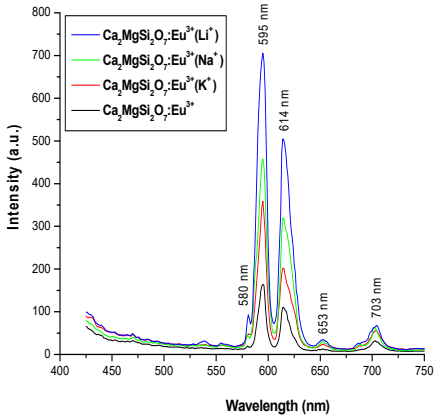

Fig. 4 (b) Emission spectra of $Ca_2MgSi_2O_7:Eu^{3+}$ and $Ca_2MgSi_2O_7:Eu^{3+}$, R^+ phosphors

The emission spectra of $Ca_2MgSi_2O_7:Eu^{3+}$ and $Ca_2MgSi_2O_7:Eu^{3+}$, R^+ phosphors were shown in Fig. 4(b) in the range of 400 to 750 nm. Under the 396 nm excitation, the emission spectrum of our obtained samples was composed of a series of sharp emission lines, corresponding to transitions from the excited states $^5D_0$ to the ground state ^7F_j (j = 0, 1, 2, 3, 4). The orange emission at about 595 nm belongs to the magnetic dipole $^5D_0 \rightarrow {}^7F_1$ transition of Eu^{3+}, and the transition hardly varies with the crystal field strength. The red emission at 614 nm ascribes to the electric dipole $^5D_0 \rightarrow {}^7F_2$ transition of Eu^{3+} ions, which is very sensitive to the local environment around the Eu^{3+}, and depends on the symmetry of the crystal field. It is found that the 595 and 614 nm emissions are the two strongest peaks, indicating that there are two Ca^{2+} sites in the $Ca_2MgSi_2O_7:Eu^{3+}$ lattice. One site, Ca (I), is inversion symmetry and the other site, Ca(II), is non-inversion symmetry. When Eu^{3+} is doped in $Ca_2MgSi_2O_7$ ions occupied the two different sites of Ca (I) and Ca (II). Other

three emission peaks located at 580, 653 and 703 nm are relatively weak, corresponding to the $^5D_0 \rightarrow ^7F_0$, $^5D_0 \rightarrow ^7F_3$ and $^5D_0 \rightarrow ^7F_4$ typical transitions of Eu^{3+} ions respectively. The strongest emission is associated to the Eu^{3+} magneti-dipole transition of $^5D_0 \rightarrow ^7F_1$, and which implies that the Eu^{3+} occupies a center of inversion asymmetry in the host lattice. For the phosphors $Ca_2MgSi_2O_7:Eu^{3+}$ and $Ca_2MgSi_2O_7:Eu^{3+}$, R^+ prepared in our experiment, the strongest orange emission peak is located at 590 nm will be dominated. It can be presumed that Eu^{3+} ions mainly occupy with an inversion symmetric center in host lattice (33). Fig. 5 shows the schematic energy level diagram of $Ca_2MgSi_2O_7:Eu^{3+}$ and $Ca_2MgSi_2O_7:Eu^{3+}$, R^+ phosphors in different emissions bands.

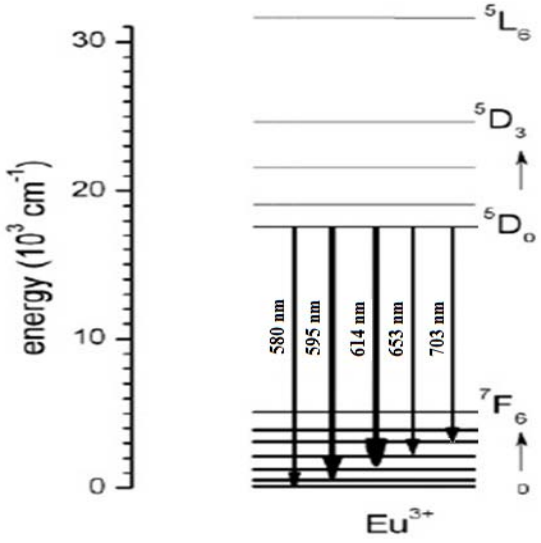

Fig. 5 Schematic energy level diagram of $Ca_2MgSi_2O_7:Eu^{3+}$ and $Ca_2MgSi_2O_7:Eu^{3+}$, R^+ phosphors

Influence of charge compensation on the luminescent intensity of $Ca_2MgSi_2O_7:Eu^{3+}$ phosphor

In the $Ca_2MgSi_2O_7:Eu^{3+}$ phosphor, ions not only play the role of activator, but also act as an aliovalent auxiliary dopant to create defects. When trivalent Eu^{3+} ions is doped into the $Ca_2MgSi_2O_7$ host, Eu^{3+} substitutes chemically, but nonequivalently, in the Ca^{2+} sites. Due to these nonequivalent substitutions, an excess of positive charge in the lattice must be compensated to maintain the electroneutrality of these phosphors. There are two possible ways to realize the charge compensation. One possible way is that two Eu^{3+} ions substitute for three Ca^{2+} ions [$2Eu^{3+} + 3Ca^{2+} \longrightarrow 2\{Eu_{Ca}\}^* + \{V_{Ca}\}''$], which creates two positive defects of $\{Eu_{Ca}\}^*$ and one vacancy defect of $\{V_{Ca}\}''$ with two electrons [$\{V_{Ca}\}'' \longrightarrow V_{Ca} + 2e\}$. The other possible charge compensation is the vacancies of Ca^{2+} [$\{V_{Ca}\}''$] created during the synthesis process. In order to improve the luminescence intensity, different charge compensation R^+ (Li^+, Na^+ and K^+) are added to $Ca_2MgSi_2O_7:Eu^{3+}$ lattice matrix (34).

As charge compensator ions R^+ (R^+ = Li^+, Na^+ and K^+) can be introduced into the host lattice of $Ca_2MgSi_2O_7:Eu^{3+}$ phosphor. The positive charge of R^+ ions neutralize the negative charge of $\{V_{Ca}\}''$, which reduces the defects of the phosphors. Fig. 5 (b) shows the emission spectra of $Ca_2MgSi_2O_7:Eu^{3+}$ and $Ca_2MgSi_2O_7:Eu^{3+}$, R^+ (R^+ = Li^+, Na^+ and K^+) phosphors. It can be seen that the co-doped Li^+, Na^+ and K^+ can all lead to the increasing luminescent intensity of Eu^{3+} ion. The reason is that Li^+, Na^+ and K^+ occupies the site of the defects and changes the symmetry of local environment of Eu^{3+} in crystal field. The luminescence intensity can be further enhanced at Li^+ charge compensation than at Na^+ and K^+ charge compensation. Since Li^+ has the least radius (0.76 Å) than Na^+ (1.02 Å) and K^+ (1.38 Å), it can be doped in the matrix more easily and help Eu^{3+} enter the host material effectively. Therefore, the improvement of the crystallinity caused by R^+ ions could be another reason for the improved PL performance (35).

3.5 CIE Chromaticity Coordinate

In general, color of any phosphor material is represented by means of color coordinates. Color coordinates are one of the important factors for evaluating phosphors performance [31]. The luminescence color of the samples excited under 395 nm has been characterized by the CIE 1931 chromaticity diagram (36). The emission spectrum of $Ca_2MgSi_2O_7:Eu^{3+}$ and $Ca_2MgSi_2O_7:Eu^{3+}$, R^+ phosphors were converted to the CIE 1931 chromaticity using the photoluminescent data and the interactive CIE software (CIE coordinate calculator) diagram as shown in Fig. 6.

Every natural color can be identified by (x, y) coordinates that are disposed inside the 'chromatic shoe' representing the saturated colors. Luminescence colors of $Ca_2MgSi_2O_7:Eu^{3+}$ and $Ca_2MgSi_2O_7:Eu^{3+}$, R^+ phosphors were placed in the orange-red (x = 0.568, y = 0.380), corners. The chromatic co-ordinates of the luminescence of this phosphor are measure and reached to orange-red luminescence.

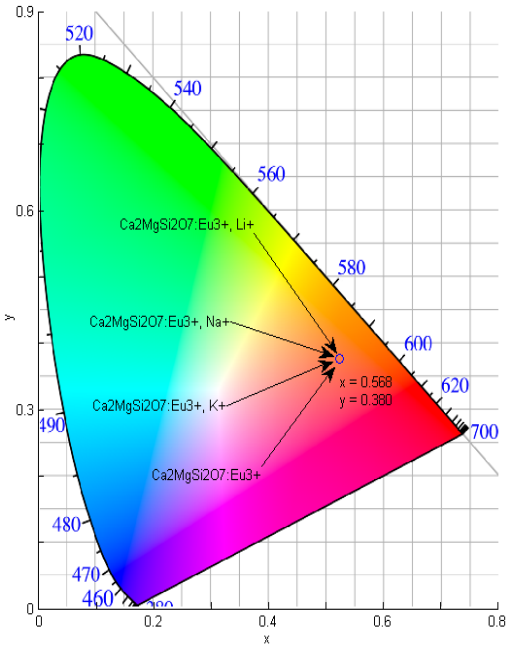

Fig. 6 CIE chromaticity diagram of $Ca_2MgSi_2O_7:Eu^{3+}$ and $Ca_2MgSi_2O_7:Eu^{3+}$, R^+ phosphors

Decay

Fig. 7 shows the typical decay curves of $Ca_2MgSi_2O_7:Eu^{3+}$, Li^+ phosphor. The initial afterglow intensity of the sample was high. The decay times of phosphor can be calculated by a curve fitting technique, and the decay curves fitted by the sum of two exponential components have different decay times.

$$I = A_1 \exp(-t/\tau_1) + A_2 \exp(-t/\tau_2) \quad (4)$$

Where, I is phosphorescence intensity, A_1, A_2 are constants, t is time, τ_1 and τ_2 are decay times (in milisecond) for the exponential components. Decay curves are successfully fitted by the equation (4) and the fitting curve result are shown. The results indicated that the, decay curves are composed of two regimes, i.e., the initial rapid decaying process and the subsequent slow decaying process.

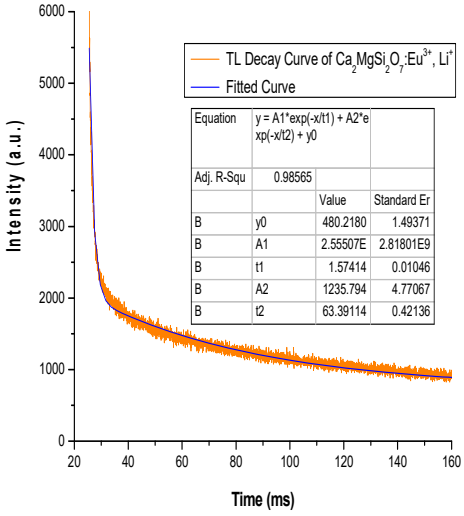

Fig. 7 Decay curves of $Ca_2MgSi_2O_7:Eu^{3+}$, Li^+ phosphor

As it was reported, when Eu^{3+} ions were doped into $Ca_2MgSi_2O_7$, they would substitute the Ca^{2+} ions. To keep electro-neutrality of the compound, two Eu^{3+} ions would substitute three Ca^{2+} ions. The process can be expressed as equation (5)

$$2Eu^{3+} + 3Ca^{2+} \longrightarrow 2\,[Eu_{Ca}]^* + [V_{Ca}]'' \quad (5)$$

Each substitution of two Eu^{3+} ions would create two positive defects of $[Eu_{Ca}]^*$ capturing electrons and one negative vacancy of $[V_{Ca}]''$. These defects act as trapping centers for charge carriers. Then the vacancy $[V_{Ca}]''$ would act as a donor of electrons while the two $[Eu_{Ca}]^*$ defects become acceptors of electrons. By thermal stimulation, electrons of the $[V_{Ca}]''$ vacancies would then transfer to the Eu^{3+} sites. The results indicate that the depth of the trap is too shallow leading to a quick escape of charge carriers from the traps resulting in a fast recombination rate in milliseconds (ms) [37].

CONCLUSIONS

In summary, $Ca_2MgSi_2O_7:Eu^{3+}$ and $Ca_2MgSi_2O_7:Eu^{3+}$, R^+ (R^+ = Li^+, Na^+ and K^+) phosphors were synthesized by high temperature solid state reaction method at 1200°C and its luminescence properties were investigated. The tetragonal crystallographies of prepared phosphors were confirmed by the XRD. PL measurements showed that the prepared phosphors exhibited emission peak with good intensity at 595 and 614 nm, corresponding to strong $^5D_0 \rightarrow {}^7F_1$ orange emission and weak $^5D_0 \rightarrow {}^7F_2$ red emission. The excitation band at 396 nm can be assigned to $^7F_0 \rightarrow {}^5L_6$ transition of Eu^{3+} ions due to the typical f–f transitions. CIE color chromaticity diagram confirms

the prepared $Ca_2MgSi_2O_7:Eu^{3+}$ and $Ca_2MgSi_2O_7:Eu^{3+}$, R^+ phosphors exhibits orange–red emission, indicating that it has favorable properties for application as near ultraviolet LED conversion phosphor. The phosphorescent life time of $Ca_2MgSi_2O_7:Eu^{3+}$, Li^+ phosphor can be calculated by a curve fitting technique, and the decay curves fitted by the sum of two exponential components have different decay times (τ_1 = 1.57 ms; τ_2 = 63.39 ms) and they possess the fast and slow decay process. The charge compensator ions R^+ ($R^+ = Li^+$, Na^+ and K^+) in $Ca_2MgSi_2O_7:Eu^{3+}$ can further enhance luminescence intensity, and the emission intensity of $Ca_2MgSi_2O_7:Eu^{3+}$ doping Li^+ is higher than that of Na^+ or K^+.

REFERENCES

1. M. Xu, L. Wang, L. Liu, D. Jia, R. Sheng, J. Lumin. **2014,** 146, 475.
2. I. P. Sahu, D. P. Bisen, N. Brahme, R. K. Tamrakar, R. Shrivastava, J. Mater. Sci.-Mater. Electron.**2016**, 26, 10075.
3. H. Y. Jiao, Y. Wang, Physica B. **2012,** 407, 2729.
4. J. Liu, K. Liang, Z. C. Wu, Y. M. Mei, S. P. Kuang, D. X. Li, Ceram. Int. **2014,** 40, 8827.
5. D. A. Steigerwald, J. C. Bhat, D. Collins, R. M. Fletcher, M. O. Holcomb, M. J. Ludowise, P. S. Martin, S. L. Rudaz, IEEE J Select Top Quant Elect **2002,** 8, 310.
6. M. Khizar, Z. Y. Fan, K. H. Kim, J. Y. Lin, H. X. Jiang, Appl Phys Lett **2005**, 86, 173504.
7. C. F. Guo, X. Ding, H. J. Seo, Z. Y. Ren, J. T. Bai, Opt Laser Technol **2011,** 43, 1351.
8. Z. C. Wu, J. Liu, W. G. Hou, J. Xu, J Alloys Compd **2010,** 498, 139.
9. I. P. Sahu, D. P. Bisen, N. Brahme, R. K. Tamrakar, J Mater Sci: Mater Electron, 27 (1) **2015,** 27 (1), 554.
10. Z. Wang, S. Lou, P. Li, J. Lumin., **2014,** 156, 87.
11. I. P. Sahu, D. P. Bisen, N. Brahme, Lumin. J. Biol. Chem. Lumin **2015,** 30 (5), 526.
12. G. J. Talwar, C. P. Joshi, S. V. Moharil, S. M. Dhopte, P. L. Muthal, V. K. Kondawat, J. Lumin. **2009**, 129, 1239.
13. I. P. Sahu, D. P. Bisen, N. Brahme, Lumin. J. Biol. Chem. Lumin. **2015,** 30(7), 1125.
14. I. P. Sahu, D. P. Bisen, N. Brahme, R. K. Tamrakar, J Mater Sci: Mater Electron, **2016,** 27(2), 1828.
15. Y. Su, L. Li, G. Li, Chem. Mater., **2008,** 20, 6060.
16. Y. Shimomura, T. Kurushima, M. Shigeiwa, N. Kijima, J. Electrochem. Soc., **2008,** 155, J45.
17. L. V. Pieterson, R. P. A. Dullens, P. S. Peijzel, A. Meijerink, G. D. Jones, J. Chem. Phys., **2001,** 115, 9393.
13. S. Okamoto, Y. Fukui, Y. Shimamura, N. Miyamoto, K. Tanaka, T. Suzuki, J. Electrochem. Soc., **2007,** 154, J383.
14. S. Shi, J. Gao, J. Zhou, Opt. Mater., **2008** 30, 1616.
15. I. P. Sahu, D. P. Bisen, N. Brahme, R. K. Tamrakar, J. Lumin. **2015,** 167, 278.
16. JCPDS file number 77-1149, JCPDS International Center for Diffraction Data.
17. R. Shrivastava, J. Saluja, Integrated Ferroelectrics, **2015,** 159, 49.
18. R. Shrivastava, J. Saluja, M. Dash, Superlattices Microstruct. 2015, 82, 262.
19. T. Rivera, C. Furetta, J. Azorín, M. Barrera, A. M. Soto, Radiat Eff. Defects Solids **2007,** 162(5), 379.
20. S. K. Gupta, M. Kumar, V. Natarajan, S. V. Godbole, Opt. Mater., **2013,** 35, 2320.
21. M. Manam, S. Das, J. Phys. Chem. Solids, **2009,** 70, 379.
22. F. M. Emen, V. E. Kafadar, N. Kulcu, A. N. Yazici, J. Lumin. **2013**, 144,133.
23. A. R. Lakshmanan, Progress in Materials Science, **1999,** 44, 1.
24. R. Chen, Y. Krish, *Analysis of Thermally Stimulated Process*, Pergamon Press, New York **1981**.
25. R. Chen, S. W. S. McKeever, *Theory of Thermoluminescence and Related Phenomenon*, World Scientific Press, Singapore **1997.**
26. H. Wu, Y. Hu, Y. Wang, F. Kang, Z. Mou, Opt. Laser Technol. **2011**, 43, 11040.
27. I. P. Sahu, Radiat Eff. Defects Solids, **2016,** 171(5–6), 511.
28. J. Liu, Z. C. Wu, P. Wang, Y. M. Mei, M. Jiang, S. P. Kuang, Lumin. J. Biol. Chem. Lumin. **2014,** 29, 868.
29. R. D. Shannon, Acta Cryst **1976,** A32, 751.
30. W. R. Liu, C. C. Lin, Y. C. Chiu, Y. T. Yeh, S. M. Jang, R. S. Liu, Opt Express **2010,** 18, 2946.
31. CIE (1931) International Commission on Illumination. Publication CIE no. 15 (E-1.3.1).
37. Y. Hong, G. Guimei, K. Li, L. Guanghuan, G. Shucai, H. Guangyan, J. Rare Earths. **2011,** 29(5), 431.